Iranian Polymer Journal (2019) 28:597–609
https://doi.org/10.1007/s13726-019-00727-1

ORIGINAL RESEARCH

A comprehensive model for the micro and meso-scale level olefin polymerization: framework and predictions

Siddharth Kulkarni[1] · **Vedprakash Mishra**[1] · **Narasimha M. Bontu**[1]

Received: 11 February 2019 / Accepted: 16 June 2019 / Published online: 22 June 2019

Abstract
A fundamental understanding of the heterogeneous olefin polymerization process is critical for imparting desired properties to the final polymer product. In this work, we have developed a comprehensive model integrating the meso-scale level intraparticle resistances to mass and heat transfer as well as the micro-scale level kinetics. The model formulation is based on the combination of the polymer flow model with the intrinsic kinetic model derived using the method of moments approach. The model is employed to study the effect of varying the mass transfer and kinetic parameters on the monomer concentration and temperature profiles inside the growing polymer macro-particle and the subsequent implications on the catalyst activity, polymer molecular weights and the polydispersity index (PDI). The simulation results showed that the steeper monomer concentration gradients in the polymer macro-particle arose on decrease of the bulk diffusivity (D_b) and increase of the number of active sites. The model also predicted the interdependence between the radial monomer concentration and temperature profiles. Further, with appropriate choice of D_b, the number of active catalyst sites, initial catalyst active site concentration and kinetic rate constants, the model predicted the catalyst activity exceeding 100 kg/g cat.hr and PDI values higher than 2. We showed that the model is capable of predicting the experimental reported polymer product properties for Ziegler–Natta, hybrid Ziegler–Natta/metallocene and supported metallocene catalyst systems.

Keywords Polyolefins · Diffusion · Heterogeneous polymers · Modeling · Method of moments

Introduction

The increased demand of polyolefins in packaging and automobile industries over last 5 decades is attributed to their easy recyclability, processability, high resistance to chemical damage, low density, and low toxicity [1, 2]. With the subsequent improvement in the catalyst activities, the reactor technologies have come a long way from the early stage high-pressure autoclave or tubular reactors to the present age low-pressure fluidized bed, loop and stirred tank reactors employing either gas, solution or slurry phase polymerization techniques [1, 3, 4]. These low-pressure technologies have also facilitated the use of co-monomers such as 1-hexene, 1-butene, and 1-octene in the polymerization process to produce polymers with tailor-made properties [1, 5].

A noteworthy progress has been made in the last 6 decades in the polyolefin production technology using various generation of Ziegler–Natta (ZN) and metallocene catalyst systems. The ZN catalysts usually consist of titanium-based compounds with organo-aluminum compounds as a co-catalyst. While titanium tetrachloride ($TiCl_4$) and diethyl aluminum chloride constitute the first generation of ZN catalysts, the second generation comprises of $TiCl_4$ supported on magnesium dichloride ($MgCl_2$) with triethyl aluminum chloride (TEAL) as a co-catalyst. The third generation of ZN catalyst consists of $TiCl_4/MgCl_2$/TEAL with ethyl benzoate and aromatic esters as internal donors (ID) and external donors (ED) to enhance the catalyst activity and stereospecificity, respectively. Subsequently, the fourth, fifth and sixth generations use the combinations of diisobutyl phthalate/silane, diether/silane and succinate/silane as ID and ED, respectively.

Electronic supplementary material The online version of this article (https://doi.org/10.1007/s13726-019-00727-1) contains supplementary material, which is available to authorized users.

✉ Narasimha M. Bontu
Narasimha.Bontu@ril.com

[1] Reaction Engineering and Modeling Group, Research and Development Department, Reliance Industries Limited, Reliance Corporate Park, Ghansoli, Navi Mumbai 400701, India

These various combinations lead to catalysts with multiple active sites and since each active site produces polymers with different average molecular weight; resulting polymer has a broad molecular weight distribution (MWD) and chemical composition distribution (CCD). On the other hand, metallocene are the single-site catalysts which form polymers with significantly narrower MWD and CCD than the ZN catalysts. These catalyst systems consist of the transition metal atoms (zirconium, hafnium, and titanium) attached to the cyclopentadienide (C_p) anions with methylaluminoxane (MAO) as co-catalysts. These highly active catalyst systems offer a more facile control over molecular architecture to produce polymers with tailor-made properties [6–8].

The modeling of the olefin polymerization processes is accomplished at three different length scales, namely; the micro-, meso-, and macro-scales using a bottom–up approach [8–10]. The micro-scale level intrinsic polymerization kinetic models are developed by neglecting the mass and heat transfer resistances, using either the population balance method (PBM) or the method of moments (MOM). The MOM approach reduces the thousands of equations of the PBM into a set of only six moment equations with three each for the living and dead polymers to determine the average molecular weight [8, 11]. The broad MWD is explained by assuming the presence of multiple catalytic active sites, each with distinct kinetic rate constants [12–14].

The single particle models (SPMs) level primarily focus on accounting for the combined heat and mass transport phenomena around a polymerizing particle coupled with a reaction term at the meso-scale level. The SPM framework inherently assumes that the final polymer particle structure is the replicate of the initial catalyst particle morphology [15].

The multigrain model (MGM) hypothesizes that the polymer macro-particle is assumed to be made up of the aggregates of the micro-particles or catalyst fragments, surrounded by the living and dead polymer chains. The MGM framework incorporates the diffusion phenomena at both the micro and macro-particle levels. The continuous generation of the polymer exerts pressure on the previously formed polymer, leading to an expansion of micro and macro-particles [15–17].

On the other hand, the polymer flow model (PFM) assumes a continuum between the catalyst fragments and growing polymer chains and neglects the heat and mass transfer limitations at the micro-particle level. The polymer phase is hypothesized to be pseudo-homogeneous and although the model serves as the limiting case of the MGM behavior, it qualitatively matches the features of MGM without compromising the physical intricacies, simplifying the numerical complexity [8, 15, 18].

Previous studies have demonstrated that the MGM and PFM frameworks with only diffusion mass transfer limitations cannot predict the high activities and the resulting high polymerization rates of these present era heterogeneous catalysts [19, 20]. The prediction capability of these models can be enhanced by integrating the monomer convective transport through the macro-particle pores in addition to the diffusive monomer transport [21–23].

In the present work, we adopt a PFM framework to describe the convection–diffusion mass transfer and heat transfer processes within a polymerizing particle and further combine the framework with the intrinsic polymerization kinetic model based on the MOM. The model serves as a useful tool to systematically understand the sensitivity of the catalyst activity (kg polymer/g cat h), polymer molecular weight and polydispersity index (PDI) to the changes in the kinetic rate constants, number of active catalyst sites, initial catalyst active site concentration (c_0^*) and the bulk diffusivity (D_b) for the Ziegler–Natta (ZN) and the supported metallocene catalyst systems. Thus, the model framework can be used to realize the limits of variations in the kinetic and mass transfer parameters to optimize the final polymer product properties. The gradients in monomer concentration and temperature across the growing polymer macro-particle as a function of D_b, initial macro-particle radius (R_0), initial catalyst fragment size (S_0), and the number of active sites can potentially provide important insights to decrease the mass transfer limitations and exothermic heat generation or minimize the hot spot formation in the reactor. We also demonstrate that the model is capable of predicting the experimental data reported in the previous literature studies for Ziegler–Natta (ZN), hybrid ZN/metallocene and supported metallocene catalyst systems used for producing polyethylene.

Model framework

Main assumptions and hypotheses

The overall model framework is based on the following important assumptions:

1. The simulations are performed for the gas phase ethylene homopolymerization in a batch reactor.
2. The mechanism of kinetics involves four steps: catalyst activation, propagation, chain transfer to the monomer followed by the catalyst deactivation.
3. The monomer concentration does not change with time on the catalyst surface during reaction but has time dependence during mass transfer from the macro-particle surface to the catalyst core.
4. The growing polymer macro-particle is constituted by the spherical micro-particles or catalyst fragments and the transport of monomer through diffusion and convec-

tion occurs through the interstitial spaces between the micro-particles (macro-particle pores).
5. The effective diffusivity (D_{eff}) accounts for the diffusive mass transport through the macro-particle pores as well as through the polymer layer surrounding active catalyst sites.
6. The effective diffusivity (D_{eff}) or the macro-particle porosity (ε) is assumed to be constant during the polymer particle growth.
7. Ideal gas law is applicable to the model framework.

Model applicability

Although unsupported metallocene catalysts are regarded as single-site, site heterogeneity has been reported for metallocene catalysts supported on inorganic carriers, which results in the broader MWD and polydispersity values higher than 2.

In particular, the study by Kou et al. [24] demonstrated that the two-site kinetic model predicts PDI and molecular weight data more accurately than the single-site model for gas-phase ethylene polymerization using metallocene catalyst supported on silica (SiO_2). Similarly, a study by Atiqullah et al. [25] predicted the existence of five different catalytically active sites for silica-supported metallocene catalyst based on the deconvolution of the MWD of polyethylene product formed. A more recent work by Moreno et al. [26] reported bimodal MWD of ethylene/1-butene and ethylene/1-hexene copolymers using chromium oxide-supported metallocene catalysts.

Moreover, the PFM framework has been previously used to explain the broad chemical composition distribution (CCD) and higher PDI values for the slurry phase copolymerization of ethylene and propylene using single-site metallocene catalysts supported on silica. The authors attributed the observed behavior to the presence of the mass transfer resistance to the growth of the polymer particles [27].

The model developed in the present work is inclusive of the meso-scale mass and heat transfer resistances as well as the multiplicity of the active catalyst sites at the micro-scale. Thus, we believe that the model framework is applicable to the Ziegler–Natta (ZN), supported metallocene and hybrid ZN/metallocene catalyst systems in particular.

Polymer flow model framework with convective mass transport

This section describes the polymer flow model (PFM) framework with the model equations and the associated boundary conditions including the convective and diffusive mass transport of the monomer through the pores. The pressure gradient developed due to monomer consumption within the macro-particle is responsible for the prevalence of the convective monomer transport. The governing equations are described as follows:

$$\varepsilon\frac{\partial[M]}{\partial t}=\frac{1}{r^2}\frac{\partial}{\partial r}\left(r^2\left(D_{\text{eff}}+p\right)\frac{\partial[M]}{\partial r}\right)-R_{\text{p}}(1-\varepsilon) \tag{1}$$

In Eq. (1), $[M]$ is the monomer concentration in the macro-particle (mol/l), ε is the macro-particle porosity, and r is the radial position in the growing polymer macro-particle. The contribution by the convective flux in Eq. (1) is given by the factor, $p\frac{\partial[M]}{\partial r}$, where, $p=\frac{k_{\text{D}}R_{\text{g}}T}{\mu_{\text{g}}}\frac{\varepsilon}{8\tau}S^2[M]$ is a dimensionless number. In this expression, k_{D} is Darcy's constant taken as unity, R_{g} is the universal gas constant (8.314 J/mol.k), μ_{g} is the monomer viscosity (Pa s), and S is the micro-particle radius (m). Also, in Eq. (1), R_{p} is the average rate of monomer consumption in the macro-particle, expressed as follows:

$$R_{\text{p}}=\sum_{j=1}^{n}k_{\text{p}}^{j}c^{*j}(t)[M] \tag{2}$$

where, c^{*j} is the catalyst active site concentration corresponding to site j. In the present work, the number of sites (n) can be either 1 or 3. The effective diffusivity is determined using the following relation:

$$D_{\text{eff}}=\frac{D_{\text{b}}\varepsilon}{\tau} \tag{3}$$

In the above relation, D_{b} is the bulk diffusivity (m^2/s), and τ is the macro-particle tortuosity.

The corresponding energy transport is given by Eq. (4) as follows:

$$\rho_{\text{p}}C_{\text{p}}\frac{\partial T}{\partial t}=\frac{1}{r^2}\frac{\partial}{\partial r^2}\left(r^2k_{\text{e}}\frac{\partial T}{\partial r}\right)+R_{\text{p}}\left(-\Delta H_{\text{rxn}}\right)(1-\varepsilon) \tag{4}$$

In Eq. (4), T, ρ_{p}, C_{p}, and k_{e} are the temperature, overall density, specific heat capacity, and thermal conductivity of the polymer mixture and ΔH_{rxn} is the heat of polymerization reaction. The evolution of micro-particle radius is given by Eq. (5) as follows:

$$\frac{\partial S}{\partial t}+u\frac{\partial S}{\partial r}=\frac{SR_{\text{p}}}{3\rho_{\text{p}}} \tag{5}$$

In the above equation, ρ_p is the polymer phase density, and u is the velocity of the polymer in the porous particle (macro-particle), which is obtained by solving the following equation:

$$\frac{1}{r^2}\frac{\partial}{\partial r}\left[(1-\varepsilon)ur^2\right]-\frac{(1-\varepsilon)R_{\text{p}}}{\rho_{\text{p}}}=0 \tag{6}$$

The growth rate of the polymer macro-particle radius (R) is equivalent to the polymer velocity in the macro-particle such that:

$$\frac{\mathrm{d}R(t)}{\mathrm{d}t} = u(R,t) \tag{7}$$

The above Eqs. (1)–(7) are solved together with single and three-site intrinsic kinetic model equations based on the method of moments (MOM) framework, described in the next section.

Method of moments framework

The method of moments (MOM) approach mainly comprises of writing the molar balance equations for the zeroth, first and second moments of the living and dead polymer chains corresponding to each of the active catalyst sites. In the current article, the model framework is developed for catalysts with single and three active sites ($j=1$ or $j=1, 2, 3$). The following partial differential equations (PDEs) are formed depending on the single-site or three-site scenarios.

For the zeroth moment of living chains:

$$\frac{\partial \mu_0^j}{\partial t} = k_a^j c^{*j}[M] - \left(k_{\mathrm{TR}}^j + k_{dac}^j\right)\mu_0^j \tag{8}$$

For the first moment of living chains:

$$\frac{\partial \mu_1^j}{\partial t} = k_a^j c^{*j}[M] - \left(k_{\mathrm{TR}}^j + k_{dac}^j\right)\mu_1^j + k_{\mathrm{p}}^j[M]\mu_0^j \tag{9}$$

For the second moment of living chains:

$$\frac{\partial \mu_2^j}{\partial t} = k_a^j c^{*j}[M] - \left(k_{\mathrm{TR}}^j + k_{dac}^j\right)\mu_2^j + k_{\mathrm{p}}^j[M]\left(2\mu_1^j + \mu_0^j\right) \tag{10}$$

For the zeroth moment of dead chains:

$$\frac{\partial \nu_0^j}{\partial t} = \left(k_{\mathrm{TR}}^j + k_{dac}^j\right)\mu_0^j \tag{11}$$

For the first moment of dead chains:

$$\frac{\partial \nu_1^j}{\partial t} = \left(k_{\mathrm{TR}}^j + k_{dac}^j\right)\mu_1^j \tag{12}$$

For the second moment of dead chains:

$$\frac{\partial \nu_2^j}{\partial t} = \left(k_{\mathrm{TR}}^j + k_{dac}^j\right)\mu_2^j \tag{13}$$

For the active catalyst sites:

$$\frac{\partial c^{*j}}{\partial t} = -\left(k_a^j[M] + k_{dac}^j\right)c^{*j} + k_{\mathrm{TR}}^j\mu_0^j \tag{14}$$

In Eqs. (8)–(14), k_{a}^j, k_{p}^j, k_{TR}^j and k_{dac}^j are the kinetic rate constants of activation, propagation, chain transfer, and catalyst deactivation for site j, respectively.

Initial and boundary condition

The initial and boundary conditions for the PFM coupled with MOM are summarized as follows:

Initial conditions:

$$t = 0, [M] = M_b,\ T = T_b,\ S = S_0,\ R = R_0,$$
$$\mu_0^j = \mu_1^j = \mu_2^j = \nu_0^j = \nu_1^j = \nu_2^j = 0,\ c^{*j} = c_0^{*j}$$
$$r = 0,\ \frac{\partial[M]}{\partial r} = 0,\ \frac{\partial T}{\partial r} = 0,\ \frac{\partial S}{\partial r} = 0,\ \frac{\partial u}{\partial r} = 0,\ \frac{\partial R}{\partial r} = 0,\ u = 0$$
$$\frac{\partial \mu_0^j}{\partial r} = \frac{\partial \mu_1^j}{\partial r} = \frac{\partial \mu_2^j}{\partial r} = \frac{\partial \nu_0^j}{\partial r} = \frac{\partial \nu_1^j}{\partial r} = \frac{\partial \nu_0^j}{\partial r} = 0$$

Boundary conditions:

$$r = R,\ D_{\mathrm{eff}}\frac{\partial[M]}{\partial r} = k_s\left([M]_{\mathrm{b}} - [M]\right),$$
$$k_{\mathrm{e}}\frac{\partial T}{\partial r} = -h\left(T - T_b\right),\ \frac{\partial S}{\partial r} = 0,\ \frac{\partial u}{\partial r} = 0,\ \frac{\partial R}{\partial r} = 0,\ \frac{\partial c^{*j}}{\partial r} = 0$$
$$\frac{\partial \mu_0^j}{\partial r} = \frac{\partial \mu_1^j}{\partial r} = \frac{\partial \mu_2^j}{\partial r} = \frac{\partial \nu_0^j}{\partial r} = \frac{\partial \nu_1^j}{\partial r} = \frac{\partial \nu_0^j}{\partial r} = 0$$

where, M_{b}, T_{b}, k_{s} and h are the bulk phase monomer concentration, bulk temperature, external mass transfer coefficient and convective heat transfer coefficient, respectively.

The above equations are solved to obtain the following important polymer properties:

$$\text{Polymer yield} = M_0\sum_{j=1}^{n}\left(\mu_1^j + \nu_1^j\right) \tag{15}$$

where, M_0 is the monomer molecular weight.

The weight average $\left(M_{\mathrm{W}}\right)$, number average molecular weights $\left(M_{\mathrm{n}}\right)$ and polydispersity index (PDI) are defined by Eqs. (16)–(18), respectively:

$$M_{\mathrm{w}} = \frac{\sum_{j=1}^{n}\left(\mu_2^j + \nu_2^j\right)}{\sum_{j=1}^{n}\left(\mu_1^j + \nu_1^j\right)} \tag{16}$$

$$M_{\mathrm{n}} = \frac{\sum_{j=1}^{n}\left(\mu_1^j + \nu_1^j\right)}{\sum_{j=1}^{n}\left(\mu_0^j + \nu_0^j\right)} \tag{17}$$

where, M_0 is the monomer molecular weight.

$$\text{Polymer PDI} = \frac{M_w}{M_n} = \frac{\sum_{j=1}^{n}\left(\mu_2^j + \nu_2^j\right)\left(\mu_0^j + \nu_0^j\right)}{\sum_{j=1}^{n}\left(\mu_1^j + \nu_1^j\right)^2} \quad (18)$$

The simulations are carried out with the help of the MATLAB software package using the 'pdepe' tool to write the partial differential equations (PDEs) and to specify the initial and boundary conditions.

Choice of simulation parameters

It is interesting to note that there exists a lack of consensus in the literature regarding the role of kinetic, mass and heat transfer parameters on influencing the polymer properties and profiles of monomer concentration and temperature across the growing polymer macro-particle radius. The present study focusses on systematically deciphering the influence of kinetic rate constants and mass transfer parameters while maintaining the heat transfer parameters constant in all the simulations. Table 1 enlists the simulation parameters used in the study.

Table 1 List of the simulation parameters used in this work

Symbol	Designation	Value
R_0	Initial macro-particle radius	10, 20, and 50 μm
S_0	Initial micro-particle radius	0.1, 0.2, and 0.5 μm
D_b	Bulk diffusivity	1×10^{-7}–1×10^{-10} m^2/s
$[M]_b$	Bulk monomer concentration	2 mol/l
c_0^{*j}	Initial catalyst active site concentration	1×10^{-5} mol/l
k_s	External mass transfer coefficient	10^{-3} m/s
k_p^j	Kinetic rate constant of propagation	100–1000 l/mol s
k_{TR}^j	Kinetic rate constant of chain transfer	0.01–1 s^{-1}
k_a^j	Kinetic rate constant of activation	0.01–1 l/mol s
k_d^j	Kinetic rate constant of deactivation	0.0001 l/mol s
T_b	Bulk temperature	343 K
h	Convective heat transfer coefficient	1 W/m^2 K
k_e	Thermal conductivity	0.005 W/m K
$-\Delta H_{rxn}$	Heat of reaction	110,000 J/mol
$\rho_p C_p$	Product of polymer density and specific heat capacity	1 J/l K[a]
ε	Macro-particle porosity	0.2
τ	Tortuosity	4
μ_g	Monomer viscosity	0.00004 Pa s[a]
ρ_p	Polymer density	25 mol/l[b]

[a]Data from NIST thermo-physical properties database

[b]Data from [23]

As indicated in Table 1, external mass transfer and convective heat transfer coefficients are significantly higher than the magnitude of corresponding diffusion–convection and heat conduction parameters such that, $D_b, p \ll k_s$ and $k_e \ll h$. These conditions ensure that mass transfer and heat transfer effects in the external film surrounding the polymer particle are negligible. The choice of the kinetic rate constants was based on previously published literature. The kinetic rate constants for each catalytic site were kept the same to equivocally understand the individual effect of k_p^j, k_{TR}^j and k_a^j. The values of R_0, bulk monomer concentration and temperature are based on typical conditions of industrial operations which are capable of producing final polymer particles of 1 mm or more.

Results and discussion

Effect of bulk diffusivity, initial macro-particle size, and micro-particle size on the radial monomer concentration and temperature profiles.

The first part of this section focusses on understanding the evolution of monomer concentration and temperature profiles inside a growing polymer macro-particle as a function of bulk diffusivity (D_b), number of sites, initial macro-particle size (R_0) and initial micro-particle size (S_0) values. Many studies have shown that the diffusive mass transfer effect becomes discernible only at $D_b < 10^{-6}$ m^2/s [19, 23]. Moreover, most of the previous literature studies used D_b or D_{eff} values below 10^{-7} m^2/s, irrespective of the type of polymerization method used such as gas phase or slurry phase polymerization [28–30]. In agreement with these studies, we also vary D_b from 10^{-7} to 10^{-9} m^2/s in our simulation study.

Figure 1a shows the effect of variation of D_b on the monomer concentration profiles across the growing macro-particle radius, obtained by solving the PFM equations with the single- and three-site intrinsic kinetic models based on MOM. All the simulations were carried out for the reaction time of 1 h. As indicated, on decreasing D_b from 10^{-7} to 10^{-9} m^2/s, the concentration of the monomer dropped more steeply from the outer surface of the polymer particle to the inner layer.

Moreover, as expected, the three-site kinetics in combination with PFM resulted in a significant decrease in monomer concentration in the polymer macro-particle, as compared to the single-site kinetics. These results imply that on decreasing D_b and increasing the number of active catalyst sites, the mass transfer effect becomes more prominent. These monomer concentration profiles with the maximum concentration at the outer macro-particle surface are indicative

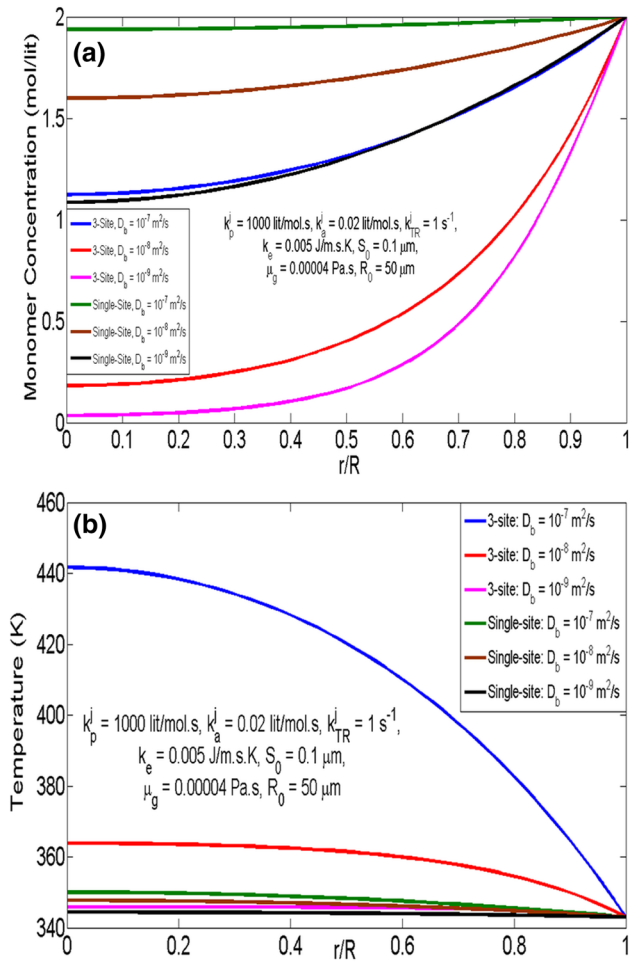

Fig. 1 Effect of bulk diffusivity (D_b) and the number of active catalytic sites on: **a** monomer concentration profiles and **b** temperature profiles across the growing polymer macro-particle (simulation parameters used are indicated on these figures)

of the inward propagation of the fragmentation front and the existence of the mass transfer resistances inside the polymer particle [31].

The results of Fig. 1a also indicate that the higher D_b or D_{eff} values, the closer is the monomer concentration at the macro-particle center to the bulk monomer concentration which is likely to increase the rate of polymerization to values comparable to the intrinsic polymerization rates. On the other hand, increasing the number of active sites has a two-fold effect: (1) it results in the more prominent mass transfer effect, characterized by the significant drop in the monomer concentration across the macro-particle radius and (2) it increases the rate of polymerization due to the availability of the more catalyst surface area for the reaction to occur. However, it is important to note that when D_b is of the order of 10^{-9} m^2/s or lower, even the three-site kinetic model combined with PFM predicts significantly low monomer concentration at the macro-particle centers (< 0.05 M_b) and consequently, polymerization rates are noticeably smaller than the intrinsic rates.

On the other hand, the single-site catalytic systems such as metallocenes are more susceptible to deactivation and reactor fouling and offer less control on the polymer morphology compared to the multi-site catalysts [32]. We propose that it is critical to understand the trade-off between D_b, the number of active catalyst sites, initial catalytic activity and process conditions while preparing the catalyst systems to attain the desired polymerization rates. The results of the present work may be potentially useful to prepare catalyst systems with the optimum ε (or D_{eff}) and the number of active sites to effectively control the final polymer product properties.

Figure 1b presents the corresponding effect on the radial temperature profiles in the polymer macro-particle. As shown, the three-site kinetic model resulted in a more significant increase in the temperature from the outer surface of the macro-particle to its center or core. It is worthwhile to note that the model in the current work is capable of capturing the interdependency between the mass and heat transfer effects as a function of D_b. As shown, at the highest value of $D_b = 10^{-7}$ m^2/s when the diffusive mass transfer effect was least pronounced, the radial temperature increase was steep from 343 K at the macro-particle surface to 441 K at the center, for the three-site intrinsic kinetic model combined with PFM.

On decreasing D_b value to 10^{-8} and 10^{-9} m^2/s, temperature rose less substantially to 364 K and 348 K, respectively. Relatively higher D_b value led to a smaller decrease in radial monomer concentration and subsequently, the term $R_p(-\Delta H_{rxn})(1-\varepsilon)$ in Eq. (4) of the energy balance became more dominant for constant values of $-\Delta H_{rxn}$ and ε, causing a more prominent increase in the temperature at the macro-particle core.

The results of Fig. 1 clearly show that drop in the monomer concentration and rise in the temperature are significant at the early stages of the polymerization since the reaction rates attain maximum and mass transfer becomes a limiting step in the initial stages of polymerization. With the progression of time, the reaction rate decreased and was lower than the mass transfer rate in the polymer layer covering the active sites. As the monomer approached the macro-particle center ($r/R \sim 0$), both rates were comparable and hence, the monomer and temperature profiles were flattened.

Further, we elucidate the effect of D_b and the number of active catalyst sites on the polymer macro-particle and catalyst micro-particle growth as a function of time, t. As shown in Fig. S1 of the supporting information, the macro-particle and micro-particle growth were more significant when the diffusion mass transfer effect was less dominant (higher D_b) and the number of active catalyst sites available were more.

In particular, the PFM coupled with three-site intrinsic kinetic model predicted an increase by a factor of 22, 16 and 8.2 in the macro-particle radius (R) for $D_b = 10^{-7}$, 10^{-8} and 10^{-9} m^2/s, respectively, over the initial R_0 of 50 µm. On replacing three-site kinetic model framework with a single-site kinetic model, the corresponding rise in R was only 8.5, 7.5 and 4.8 times (Fig. S1(a), supporting information). Qualitatively, similar profiles were observed for the micro-particle radius, S as a function of D_b and the number of active sites [Fig. S1(b), supporting information].

In summary, our results suggested that the higher the D_b value and more the number of active catalyst sites, more pronounced was the growth of polymer macro-particle and catalyst fragments. Our results were consistent with the simulation results of the work of Nouri et al. [29], which demonstrated that at lower $\theta = \frac{Rk_pC_0^*}{D_{eff}}$ or higher D_{eff} values, the polymer particle grew more significantly.

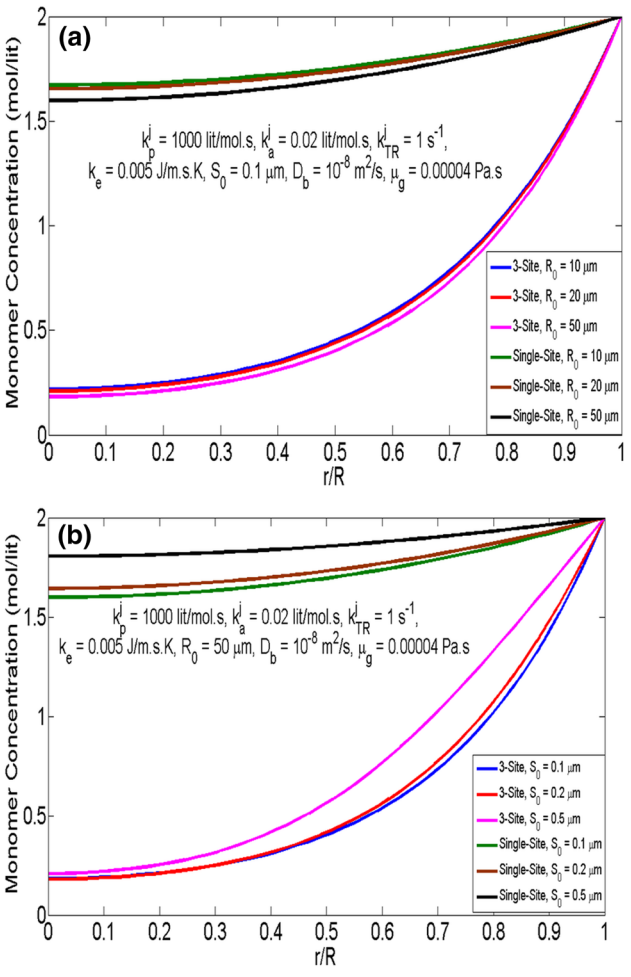

Fig. 2 Effect of variation of: **a** initial macro-particle size (R_0) and **b** initial micro-particle size (S_0) on radial monomer concentration profiles (simulation parameters used are indicated on these figures)

The monomer from the surface of the polymer particle has to diffuse through the polymeric pores to get adsorbed on the polymer layer surrounding the catalyst fragments followed by the diffusion through this layer to reach the active sites, where the reaction occurs. At the lower values of D_b, the monomer appears to encounter more resistance through the pores and previously formed polymer layers to reach the active catalytic sites and subsequently, the macro and micro-particle growth is hindered.

On the other hand, when a higher number of active sites are available to the monomer, conditions are more favorable for the polymerization reaction, and subsequently, R and S grow more prominently. It is important to note that for the simulation results of Fig. 2, the convective mass transfer parameters were unchanged while varying D_b and therefore, the observed trends in S and R values were governed primarily by the diffusive mass transfer.

Figure 2 illustrates the effect of variation of R_0 and S_0 on the radial monomer concentration profiles at $D_b = 10^{-8}$ m^2/s for the single- and three-site scenarios. As evident from Fig. 2a, a larger R_0 value led to a more pronounced drop in the monomer concentration, regardless of the number of active sites. These profiles indicated that at larger value of R_0, increased intraparticle diffusional limitations were encountered for the given set of convective mass transfer parameters, resulting in the increase of monomer consumption inside the polymer macro-particle. Since the final polymer particle morphology resembles the morphology of the catalyst particle within the SPM framework, we hypothesized that the catalyst batch comprising of the majority of the larger sized particles is likely to experience more substantial mass transfer resistances than the smaller sized particles. Consequently, a more significant deviation from the intrinsic rates occurred for the polymerization rates. Our hypothesis was supported by various previous simulation studies [33, 34]. A recent experimental work by Bashir et al. [35] also demonstrated that smaller particle size of silica supported metallocene catalyst led to high initial polymerization rates and productivity in the slurry and gas phase homo and copolymerization of ethylene.

The time required by the monomer to diffuse through the porous particle is reported to be directly proportional to the square of the particle radius. Hence, the residence time of the catalyst/polymer particle with a larger initial size is higher than the smaller sized particles for a given polymerization rate or monomer conversion. It is probable that the active sites of the larger catalyst particles with longer residence time are deprived of the incoming monomer molecules, thereby reducing the efficiency of polymerization [35]. We speculate that these conditions may lead to the formation of the fine particles in the reactor especially when the polymerization reaction rates are significantly higher.

Interestingly, when the particle size is very small, there exists a possibility of agglomeration, segregation, non-uniform mixing of the polymer particles and subsequent deposition on the equipment surface and reactor walls. Thus, prior to the process operations, it is essential to ensure that the initial catalyst particle size or particle size distribution is selected optimally to avoid increasing reactor size unreasonably to provide for the large residence times and also to avoid build-up of agglomerates.

Remarkably, a rise in the initial catalyst fragment or micro-particle size (S_0) has an opposite effect on the radial monomer concentration profiles, for a given D_b value. As shown in Fig. 2b, higher the S_0 value, less substantial are the monomer concentration gradients across the macro-particle. These simulation results can be attributed to the increase in the convective mass transfer effect with an increase in S_0. We believe that at higher S_0 value, the term $p = \frac{k_D R_g T}{\mu_g} \frac{\varepsilon}{8\tau} S^2[M]$ is numerically significant and comparable to that of D_{eff}. In particular, for S_0=0.1–0.5 μm, p$\approx 10^{-8}$ m^2/s which is almost equivalent to $D_{eff} = 10^{-8} \times \frac{0.2}{4}$.

In summary, the model predictions showed that the inclusion of the convection term in the model framework resulted in an overall decrease in the mass transfer limitations and subsequently, increased reaction rates. These results are concomitant with the observations of Veera et al. [36] and Liu [37].

The subsequent effect on the radial temperature profiles is shown in Fig. S2 in the supporting information. The temperature increase from the macro-particle surface to its core was more discernible at higher R_0 as shown in Fig. S2(a). On the other hand, when S_0 increased from 0.1 to 0.5 μm, the temperature gradient was more distinct, the effect was more noticeable for the three-site kinetic model coupled with PFM (Fig. S2(b), supporting information).

We hypothesize that with an increase in the S_0 value, the convective mass transfer effect became more prominent resulting in a higher monomer concentration which led to an increase in the magnitude of the term $R_p(-\Delta H_{rxn})(1-\varepsilon)$ in the energy balance equation, resulting in a significantly large temperature gradient across the polymer micro-particle. Thus, higher R_0 and S_0 values led to a higher temperature at the polymer macro-particle core and subsequently, more exothermic heat generation inside the polymerizing particle.

Figures 1 and 2 illustrate how the diffusive and convective mass transfer parameters and multiplicity of the active catalyst sites influence the meso-scale level monomer concentration and temperature profiles. We now attempt to decipher the subsequent effect of these parameters and the kinetic rate constants on the polymer properties. Firstly, we determined the catalyst activity (kg polymer/g cat h) by dividing the polymer yield per hour by the quantity of catalyst. The influence of variation of D_b, the number of active sites and kinetic rate constants of propagation, activation and chain transfer were interpreted based on the simulation results.

The high initial polymerization rates corresponding to higher D_b and k_p values also increased the corresponding temperatures and heat transfer rates; causing heat accumulation inside the growing polymer macro-particles. The increased heat accumulation may lead to the faster propagation, increased chain transfer and deactivation of active sites relative to the catalyst activation, giving rise to the particle agglomeration and consequently, reactor fouling [35]. Hence, robust heat removal and temperature control system is imperative to ensure that monomer reaches the active sites prior to pronounced deactivation and contamination and to further reduce the possibility of the occurrence of the thermal reaction runaway scenarios. The reactor may be operated in a narrow temperature

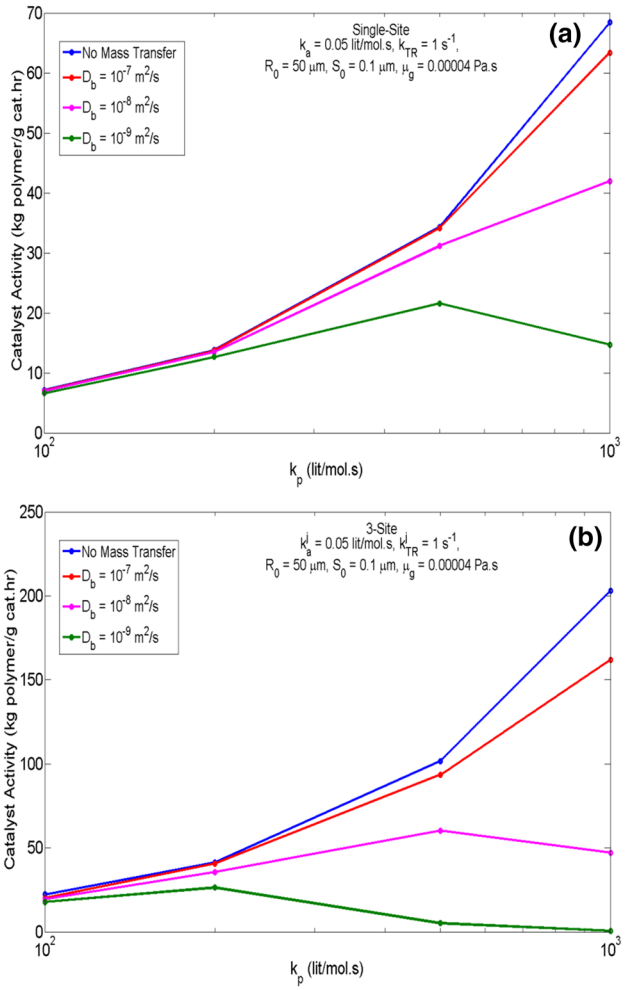

Fig. 3 Effect of variation of kinetic rate constant of propagation (k_p) and bulk diffusivity (D_b) on the catalyst activity in kg polymer/g cat h for: **a** the single-site and **b** three-site kinetic models combined with PFM (simulation parameters used are indicated on these figures)

range to warrant stable operation, particularly for the gas phase polymerization.

Effect of bulk diffusivity and kinetic rate constant of propagation on the catalyst activity

Figure 3 shows the catalyst activity as a function of bulk diffusivity (D_b) and kinetic rate constant of propagation (k_p^j) parameters for the single and three-site scenarios. As indicated, the three-site kinetic model in combination with PFM predicted higher catalyst activity than the single-site model for the same set of kinetic, mass and heat transfer parameters. Moreover, as the mass transfer resistance was prominent with decreasing D_b, the catalyst activity decreased, as well.

It is interesting to note that the catalyst activity bears a non-monotonic trend with k_p^j. These results suggest that for the given set of simulation parameters, it is critical to determine the optimum values of k_p^j and D_{eff}, yielding the maximum catalyst activity and high polymerization rates. Figures 3a and b further indicate that polymerization capacity in excess of 100 kg/g cat h can be achieved for $D_b = 10^{-7}$ m^2/s ($D_{eff} \approx 0.5 \times 10^{-8}$ m^2/s) and $k_p^j > 500$ l/mol s, when three-site kinetic model coupled with PFM was used in place of the single-site model.

We now attempt to study the time evolution of PDI by combining the single and three-site intrinsic kinetic models with the PFM as a function of D_b and k_p^j at fixed values of k_{TR}^j and k_a^j.

Effect of variation of bulk diffusivity and kinetic rate constant of propagation on the polymer polydispersity index

The polydispersity index (PDI), which is the ratio of weight average and number average molecular weight of the formed polymer, provides insights about the broadness of molecular weight distribution (MWD) and serves as the quantitative measure of the inhomogeneity of the distribution. In general, higher PDI is an indicator of the broader MWD. The polymer PDI has important implications on the polymer processing, particularly during extrusion and spinning of the polymer into filaments. Furthermore, the PDI also influences the polymer properties such as the melt fracture performance, viscoelastic behavior and toughness [38–40].

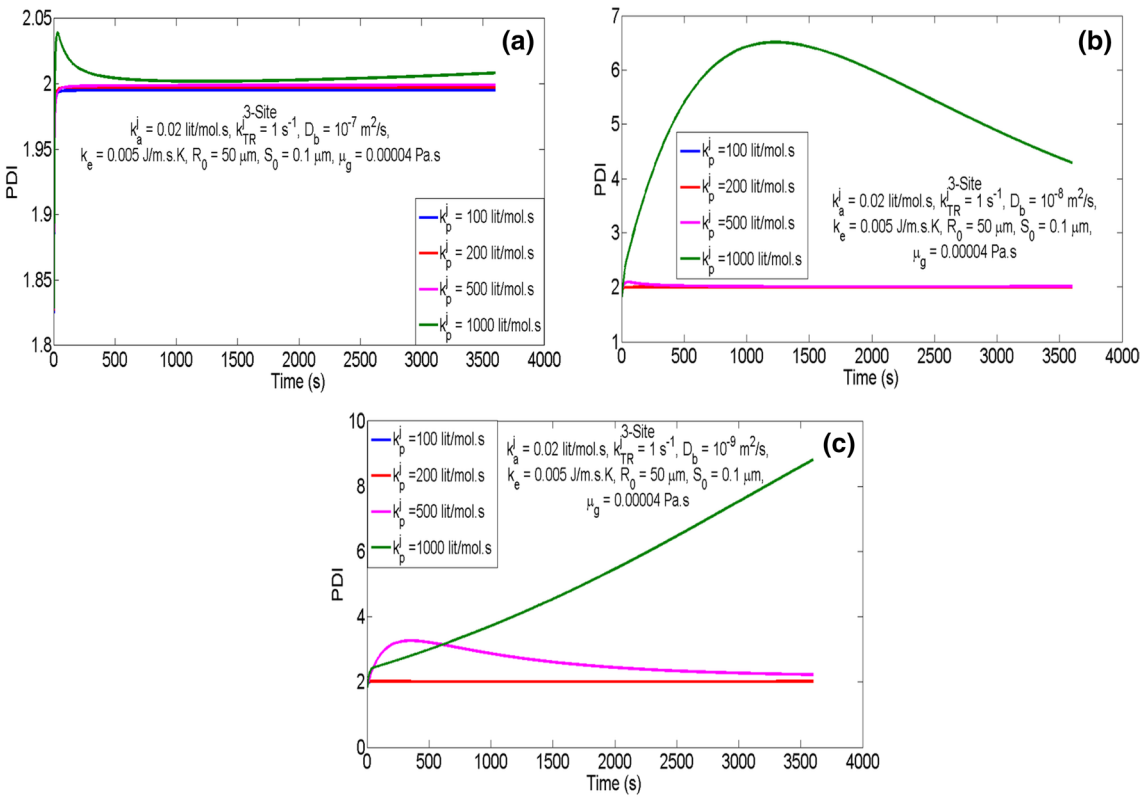

Fig. 4 Effect of variation of k_p^j and D_b on the polydispersity index (PDI) as a function of time for the three-site kinetic model coupled with PFM: **a** $D_b = 10^{-7}$ m^2/s, **b** $D_b = 10^{-8}$ m^2/s and **c** $D_b = 10^{-9}$ m^2/s (simulation parameters used are indicated on these figures)

Figure 4 presents the influence of k_p^j on the PDI at different D_b values for the three-site kinetic model coupled with PFM, respectively. The model framework predicted PDI ≈ 2 for the three-site kinetic model coupled with PFM when the mass transfer effect was less dominant at $D_b = 10^{-7}$ m^2/s (Fig. 4a). On decreasing D_b to 10^{-8} m^2/s, PDI increased until $t = 1300$ s, attained a maximum value of 6.8 and then dropped to reach a final value ~ 4.6 at $t = 3600$ s, corresponding to $k_p^j = 1000$ l/mol s for the three-site scenario (Fig. 4b). On the other hand, when single-site kinetic model was replaced by three-site kinetic model, PDI values ~ 8 can be predicted at high $k_p^j = 1000$ l/mol.s corresponding to $D_b = 10^{-9}$ m^2/s (Fig. 4c).

Our results indicated that when the mass transfer resistances were included, the monomer concentration on the outer surface of the polymer micro-particle was different from the concentration at the center. This gradient in the monomer concentration resulted in the production of polymer with different molecular weights (broad MWD) and PDI higher than 2.

Moreover, the broad MWD or high PDI are reported to be a consequence of the difference in the nature of active catalyst sites, arising from the multiplicity of the active sites and the difference in kinetic rate constants for each site. Many previous studies showed that PDI higher than 2 can be predicted by assuming the multiple active sites with negligible mass transfer limitations [13, 41]. The combination of the intrinsic kinetic model with the single particle model frameworks was also capable of predicting high PDIs or broad MWD [42–44].

The studies employing the multi-site intrinsic kinetic models with no mass and heat transfer effects used different kinetic rate constants for each present work, we elucidated the implication of independently varying k_p^j, k_{TR}^j, etc. and maintaining the same set of constants for each active catalyst site on the polymer properties in the presence of mass and heat transfer limitations. We believe that these results will act as a guide for many future experimental studies focusing on unraveling the kinetics and effect of operating conditions on the olefin polymerization.

Sensitivity analysis of model parameters- influence on final polymer properties

We now present the sensitivity analysis of these model parameters to understand their influence on the final polymer product properties. The sensitivity analysis is useful to determine the maximum or minimum limit of these parameters beyond which the change in the value of these parameters have an undesirable effect on the polymer properties. The influence of variations of k_p, D_b, number of catalyst active sites, k_{TR} and c_0^* values on weight average molecular weight (M_w), number average molecular weight (M_n), PDI, catalyst activity and final rate of polymerization are summarized in Tables S1–S5 of the supporting information.

Increasing k_p increased the rate of polymerization (R_p) (Eq. 2) which was likely to result in the sharper drop in the monomer concentration across the growing polymer particle (Eq. 1). On the other hand, the rate of formation of living chains also increased with an increase in k_p value (Eqs. 8–10). The higher the number of available catalyst active sites, the more predominant is the increase in the concentration of living polymer chains accompanied by lower monomer concentration at the macro-particle center which resulted in the lower rates of polymerization. As shown in Table S1 of the supporting information, the catalyst activity, M_w, M_n and polymerization rates increased monotonically with k_p for $D_b = 10^{-8}$ m^2/s for the single and two-site kinetic model coupled with PFM. However, these properties exhibited a decrease beyond $k_p^j = 500$ l/mol s when three-site kinetic model was combined with PFM. Thus, we propose that increasing k_p value and the number of active catalyst sites do not always have a favorable influence on the polymer properties. The resultant polymer properties were also depended on D_b, as evident from Tables S2 of the supporting information. We showed that only by increasing D_b from 10^{-8} to 10^{-7} m^2/s, the polymer properties varied monotonically with k_p values even for the three-site kinetic model in combination with PFM.

As shown in Table S3 of the supporting information, decreasing D_b value led to an increase in the diffusive mass transfer contribution and more significant decrease in the monomer concentration from the bulk to the center of the macro-particle and consequently, the catalyst activity, polymer molecular weights and rate of polymerization decrease. A decrease in D_b value also resulted in an increase in PDI, the effect being more significant for two and three-site scenarios, which indicated that number of catalyst sites as well as the extent of mass transfer effect, were responsible for higher PDI values.

An increase in k_{TR} favoured formation of dead polymer chains and suppressed the formation of living chain as suggested by Eqs. (8)–(13). Thus, the catalyst activity and polymer molecular weights dropped with an increase in k_{TR} value. As indicated by Eqs. (14) and (2), the catalyst active site concentration (c^*) and consequently, the polymerization rate depend upon the product of k_{TR} and the zeroth moment of living chains (μ_0). While μ_0 decreased with an increase in k_{TR} value according to Eq. (8), c^* was likely to increase with an increase in k_{TR}(Eq. 14). Subsequently, the polymer properties have a non-monotonic dependence on k_{TR}, particularly for two and three-site kinetic models combined with PFM. The results are summarized in Table S4 of the supporting information.

An increase in the initial catalyst active site concentration (c_0^*) resulted in higher value of c^*, which increased the rate of polymerization and caused a prominent drop in monomer concentration across the growing polymer macro-particle (Eq. 2). On the other hand, an increase in the value of c^* led to higher concentration of living polymer chains (Eqs. 8–10). The resultant polymer properties were likely to be governed by these two opposing effects. Our results are summarized in Table S5 of the supporting information which show that below $c_0^* = 10^{-6}$ mol/l, polymer properties are not influenced significantly probably due to an equal contribution by Eqs. (2) and (8)–(10).

In summary, our results demonstrated that the final polymer properties are the complex function of model parameters and do not always change monotonically with the variation in k_p, k_{TR}, and c_0^* values and the number of active sites.

Model validation with experimental data

The model framework was validated against the experimental data of the following two cases:

1. Ochędzan-Siod£ak and Nowakowska [45] used three different titanium ($TiCl_4$) catalysts immobilized on the $MgCl_2$/tetrahydrofuran (THF)/diethyl aluminum chloride/triethyl aluminum ($AlEt_3$) co-catalyst to produce polyethylene. Interestingly, the authors proposed that all the three catalyst systems are single-site, based on the properties of the final polyethylene product. We have validated experimental catalyst activity and the weight average molecular weight (M_w) by combining the single-site kinetic model with the polymer flow model (PFM).
2. Ahmadi et al. [46] employed ZN/metallocene hybrid catalyst for producing bimodal polyethylene. We have validated the experimental data of catalyst activity and polymer yield using two and three-site kinetic models in combination with PFM.

To validate the experimental results of cases (1) and (2), we have neglected the monomer convection flux contribution in Eq. (1) of the main manuscript.

3. Bashir et al. [35] investigated the effect of particle size of silica-supported metallocene/methylaluminoxane (MAO) catalysts on the final polymer properties in gas and slurry-phase ethylene polymerization. We have validated the experimental data of weight average molecular weight (M_w) and PDI for the gas phase polymerization of ethylene by including the convective flux term (i.e., Eq. 1) in the model equations. Since the authors indicate that the PDI values greater than two are likely to be due to the presence of multiple catalytic active sites and/or the mass transfer resistances in catalyst particles to the monomer transport, we have used a two-site kinetic model in combination with PFM. It is important to note that the catalyst samples selected for validation (BG-1, BG-2, and BG-3) have almost the identical composition of aluminum (Al) and zirconium (Zr) and comparable pore diameter and specific surface area.

Tables S6–S10 in the supporting information summarize the validation results and the kinetic/mass transfer parameters used in the simulations.

Our results are in good agreement with the experimental data of catalyst activity, polymer yield and average polymer molecular weight. We showed that the three-site kinetics leads to a better prediction of the experimental polymer properties than the two-site kinetics combined with PFM, for the model validation study of case (2). As evident from Table S8 of the supporting information, once the kinetic rate constants and D_b are fixed for run 5 to determine the catalyst activity, the same set of parameters predict the time dependent polymer yield with a maximum deviation of only 4% from the experimental data (Table S9), indicative of the appropriate tuning of the model parameters.

It is worthwhile to note that for predicting the polymer properties for validation study of case (3), we have assumed the same set of kinetic/mass transfer parameters owing to the similar composition and specific surface area of the catalyst samples and identical temperature/pressure conditions for polymerization. Interestingly, as shown in Table S10 (supporting information), the model predictions match with the experimental data satisfactorily. The small deviation from the experimental data is probably due to the same value of D_b used in the simulations. The larger catalyst particle size was reported to give rise to more prominent mass transfer limitations to the monomer transport for reaching the catalyst-active sites and thus, may have a lower value of D_b [35].

Conclusion and outlook

In the present work, a comprehensive model framework was developed which combined the meso-scale level convective–diffusive mass transport and energy transport with the micro-scale level intrinsic polymerization kinetics as a function of bulk diffusivity, the number of active catalyst sites, initial polymer macro-particle size, catalyst micro-particle size, the kinetic rate constants and initial active site concentration. The model is capable of predicting the monomer concentration and temperature profiles within the growing polymer macro-particle together with the micro-scale polymer properties

such as catalyst activity, molecular weight, PDI and rates of polymerization. The inclusion of the convective monomer mass transport decreased the radial monomer concentration gradient and consequently, limited the effect of the diffusive mass transport on the catalyst activity. We showed that with the suitable tuning of the meso-scale mass transfer and micro-scale kinetic parameters, the catalyst activity and PDI comparable with the present-day high -activity catalysts can be estimated. The sensitivity analysis of the model parameters indicated that the resultant polymer properties varied non-monotonically with the kinetic rate constant of propagation, chain transfer and the number of active catalyst sites, mainly when bulk diffusivities were of the order of 10^{-8} m^2/s or lower. The model predictions were in good agreement with the experimental data of Ziegler–Natta and hybrid Ziegler–Natta/metallocene catalyst systems for producing polyethylene. Although the present modeling framework was developed for the gas phase homopolymerization of ethylene in a batch reactor, it can be easily extended to slurry and gas/liquid phase homo and copolymerization of olefins in different reactor systems including the semi-batch, fluidized bed and continuous stirred tank reactors with minor modifications in the model equations. We also believe that the results furnished from the present work have the potential to improve the current understanding of the micro-scale and meso-scale level modeling of the heterogeneous polymerization process which can serve as the foundation for the macro-scale reactor level modeling to determine the residence time/flow distribution for the reliable reactor scale-up and operations. Further validation of the model framework is underway to predict the results presented in the work of Hakim et al. [47] using Ziegler–Natta catalyst to predict average molecular weight, MWD, PDI and residence time for ethylene copolymerization in the slurry phase.

References

1. Chum PS, Swogger KW (2008) Olefin polymer technologies—history and recent progress at the Dow Chemical Company. Prog Polym Sci 33:797–819
2. Sauter WD, Taoufik M, Boisson C (2017) Polyolefins, a success story. Polymers 9:185–197
3. Whiteley KS, Heggs TG, Koch H, Mawer RL, Immel W (2000) Polyolefins—Ullmann's encyclopedia of industrial chemistry. Wiley, Weinheim
4. Galli P, Vecellio G (2004) Polyolefins: the most promising large-volume materials for the 21st century. J Polym Sci Polym Chem 42:396–415
5. Ittel SD, Johnson LK, Brookhart M (2000) Late-metal catalysts for ethylene homo- and copolymerization. Chem Rev 100:1169–1204
6. Chadwick JC, Garoff T, Severn JR (2008) In: Severn JR, Chadwick JC (eds) Tailor-made polymers: via immobilization of alpha-olefin polymerization catalysts. Wiley, Weinheim
7. Fan ZQ, Yu Y (2018) Ziegler–Natta catalysts. Encycl Polym Sci Technol 2018:1–24
8. Soares JBP, McKenna T, Cheng CP (2007) In: Asua J (ed) Polymer reaction engineering. Blackwell, Oxford
9. Zhu Y-P, Chen G-Q, Luo Z-H (2014) Particle behavior in FBRs: a comparison of the PBM–CFD, multi-scale CFD simulation of gas–solid catalytic propylene polymerization. Macromol React Eng 8:609–621
10. McKenna TF, Soares JBP (2001) Single particle modelling for olefin polymerization on supported catalysts: a review and proposals for future developments. Chem Eng Sci 56:3931–3949
11. Mastan E, Zhu S (2015) Method of moments: a versatile tool for deterministic modeling of polymerization kinetics. Eur Polym J 68:139–160
12. Ahmadi M, Nekoomanesh M, Arabi H (2010) A simplified comprehensive kinetic scheme for modeling of ethylene/1-butene copolymerization using Ziegler–Natta catalysts. Macromol React Eng 4:135–144
13. Nassiri H, Arabi H, Hakim S (2012) Kinetic modeling of slurry propylene polymerization using a heterogeneous multi-site type Ziegler–Natta catalyst. React Kinet Mech Catal 105:345–359
14. Abbasi MR, Shamiri A, Hussain MA (2016) Dynamic modeling and molecular weight distribution of ethylene copolymerization in an industrial gas-phase fluidized-bed reactor. Adv Powder Technol 27:1526–1538
15. Soares JBP, McKenna TF (2012) Polyolefin reaction engineering. Wiley, Weinheim
16. Casalini T, Visscher F, Tamaddoni M, Friederichs N, Bertola F, Storti G, Morbidelli M (2018) The effect of residence time distribution on the slurry-phase catalytic ethylene polymerization: an experimental and computational study. Macromol React Eng 12:1700058
17. Alizadeh A, McKenna TF (2018) Particle growth during the polymerization of olefins on supported catalysts. Part 2: current experimental understanding and modeling progresses on particle fragmentation, growth, and morphology development. Macromol React Eng 12:1700027
18. McKenna TF, Bashir MA (2019) In: Albunia AR, Prades F, Jeremic D (eds) Multimodal polymers with supported catalysts: design and production. Springer, Basel
19. McKenna TF, Dupuy J, Spitz R (1997) Modeling of transfer phenomena on heterogeneous Ziegler catalysts. III. Modeling of intraparticle mass transfer resistance. J Appl Polym Sci 63:315–322
20. Weickert G, Meier GB, Pater JTM, Westerterp KR (1999) The particle as microreactor: catalytic propylene polymerizations with supported metallocenes and Ziegler-Natta catalysts. Chem Eng Sci 54:3291–3296
21. McKenna TF, Dupuy J, Spitz R (1995) Modeling of transfer phenomena on heterogeneous Ziegler catalysts: differences between theory and experiment in olefin polymerization (an introduction). J Appl Polym Sci 57:371–384
22. Kittilsen P, Svendsen H, McKenna TF (2001) Modeling of transfer phenomena on heterogeneous Ziegler catalysts. IV. Convection effects in gas phase processes. Chem Eng Sci 56:3997–4005
23. Veera P, Weickert G, Agarwal US (2002) Modeling monomer transport by convection during olefin polymerization. AIChE J 48:1062–1070
24. Kou B, McAuley KB, Hsu CC, Bacon DW, Yao KZ (2005) Mathematical model and parameter estimation for gas phase ethylene homopolymerization with supported metallocene catalysts. Ind Eng Chem Res 44:2428–2442
25. Atiqullah M, Cibulková Z, Černá A, Šimon P, Hussain I, Al-Harthi MA, Anantawaraskul S (2015) Effects of supported metallocene catalyst active center multiplicity on antioxidant-stabilized ethylene homo- and copolymers. J Therm Anal Calorim 119:581–595

26. Moreno J, Paredes B, Carrero A, Vélez D (2017) Production of bimodal polyethylene on chromium oxide/metallocene binary catalyst: evaluation of comonomer effects. Chem Eng J 315:46–57
27. Hoel EL, Cozewith C, Byrne GD (1994) Effect of diffusion on heterogeneous ethylene propylene copolymerization. AIChE J 40:1669–1684
28. McKenna TF, Cokljat D, Spitz R, Schweich D (1999) Modelling of heat and mass transfer during the polymerization of olefins on heterogeneous Ziegler catalysts. Catal Today 48:101–108
29. Nouri M, Parvazinia M, Arabi H (2015) Effect of fragment size distribution on reaction rate and molecular weight distribution in heterogeneous olefin polymerization. Iran Polym J 24:437–448
30. Li H, Che L, Luo Z (2014) Modeling intraparticle transports during propylene polymerizations using supported metallocene and dual function metallocene as catalysts: single particle model. Chem Ind Chem Eng Q 20:249–260
31. Merquior DM, Lima EL, Pinto JC (2005) Modeling of particle fragmentation in heterogeneous olefin polymerization reactions, 2. Macromol Mater Eng 290:511–524
32. Katia T, Soares JBP (2002) Gas-phase polymerization of ethylene using supported metallocene catalysts: study of polymerization conditions. Macromol Chem Phys 203:1895–1905
33. Yiagopoulos A, Yiannoulakis H, Dimos V, Kiparissides C (2001) Heat and mass transfer phenomena during the early growth of a catalyst particle in gas-phase olefin polymerization: the effect of prepolymerization temperature and time. Chem Eng Sci 56:3979–3995
34. Kanellopoulos V, Dompazis G, Gustafsson B, Kiparissides C (2004) Comprehensive analysis of single-particle growth in heterogeneous olefin polymerization: the random-pore polymeric flow model. Ind Eng Chem Res 43:5166–5180
35. Bashir MA, Monteil V, Boisson C, McKenna TF (2017) Experimental proof of the existence of mass-transfer resistance during early stages of ethylene polymerization with silica supported metallocene/MAO catalysts. AIChE J 63:4476–4490
36. Veera PU (2003) Mass transport models for a single particle in gas-phase propylene polymerization. Chem Eng Sci 58:1765–1775
37. Liu X (2007) Modeling and simulation of heterogeneous catalyzed propylene polymerization. Chin J Chem Eng 15:545–553
38. Ansari M, Derakhshandeh M, Doufas AA, Tomkovic T, Hatzikiriakos SG (2018) The role of microstructure on melt fracture of linear low density polyethylenes. Polym Test 67:266–274
39. Hatzikiriakos SG (2000) Long chain branching and polydispersity effects on the rheological properties of polyethylenes. Polym Eng Sci 40:2279–2287
40. Sadeghi F, Ajji A (2013) Effect of molecular structure on seal ability, flex crack and mechanical properties of linear low-density polyethylene films. J Plast Film Sheeting 30:91–111
41. Chen K, Mehdiabadi S, Boping L, Soares JBP (2016) Estimation of apparent kinetic constants of individual site types for the polymerization of ethylene and α-olefins with Ziegler–Natta catalysts. Macromol React Eng 10:551–566
42. Dashti A, Ramazani A (2008) Modeling and simulation of olefin polymerization at microstructure level. Iran J Chem Chem Eng 27:13–22
43. Najafi M, Parvazinia M (2015) Computational modeling of particle fragmentation in the heterogeneous olefin polymerization. Macromol Theory Simul 24:28–40
44. Casalini T, Visscher F, Janssen E, Bertola F, Storti G, Morbidelli M (2017) Modeling of polyolefin polymerization in semibatch slurry reactors: experiments and simulations. Macromol React Eng 11:1600036
45. Ochędzan-Siodłak W, Nowakowska M (2007) Titanium catalyst ($TiCl_4$) supported on $MgCl_2(THF)(AlEt_2Cl)_{0.34}$ for ethylene polymerization. Polimery 52:184–189
46. Ahmadi M, Jamjah R, Nekoomanesh M, Zohuri GH, Arabi H (2007) Ziegler-Natta/metallocene hybrid catalyst for ethylene polymerization. Macromol React Eng 1:604–610
47. Hakim S, Moballegh L (2006) Simulation of a series of industrial slurry reactors for HDPE polymerization process using deconvolution of the GPC graph of only the first reactor. Iran Polym J 15:655–666